Physics and Chemistry of Minerals (2024) 51:35
https://doi.org/10.1007/s00269-024-01295-4

ORIGINAL PAPER

Raman spectroscopic study of liebenbergite and Ni_2SiO_4 spinel at high pressure and high temperature: nickel effects on the vibration properties of olivine and spinel structures

Shuchang Gao[1,2] · Jinpu Liu[1] · Hang Cheng[1,2] · Li Zhang[1] · Yanhao Lin[2] · Xiaoguang Li[3] · Xueqing Qin[4]

Received: 29 January 2024 / Accepted: 31 July 2024 / Published online: 26 August 2024

Abstract

High-pressure and high-temperature Raman spectroscopic measurements of synthetic liebenbergite and Ni_2SiO_4 spinel have been conducted up to 22 GPa and 700 °C, respectively. Isothermal and isobaric mode Grüneisen parameters were calculated based on the observed Raman modes. The intrinsic anharmonicities of liebenbergite and Ni_2SiO_4 spinel were also evaluated. The changes of the asymmetric SiO_4 stretching band of Ni_2SiO_4 spinel in frequency are irreversible under decompression, indicating a potential pressure-induced modification in the crystal structure at elevated pressures. The values of isothermal mode Grüneisen parameters show that the SiO_4 internal vibrations in Ni-rich olivines are more sensitive to the variations of pressure. For spinel-group minerals, the SiO_4 internal vibrations can be less sensitive to the pressure change due to nickel incorporation. In contrast, according to the values of isobaric mode Grüneisen parameters, nickel increases the sensitivity of these vibrations to the variations of temperature. In addition, nickel has distinctive effects on the intrinsic anharmonicities of different vibration modes in both olivine and spinel-group minerals, and therefore alter the thermodynamic properties of their crystal structures.

Keywords Liebenbergite · Ni_2SiO_4 spinel · High-pressure and high-temperature Raman spectroscopy · Grüneisen parameter · Intrinsic anharmonicity

Introduction

The olivine (M_2SiO_4, M = divalent cation) orthosilicate and its high-pressure polymorphs are important phases of the Earth's interior. In the upper mantle, $(Mg, Fe)_2SiO_4$ olivine (α-phase) is believed to be the most abundant mineral. It transforms to wadsleyite (β-phase) at 410-km depth and then to ringwoodite (γ-phase) at a depth of about 520 km in the mantle transition zone (Ringwood and Major 1970; Kohlstedt et al. 1996; Redfern et al. 2000; Chudinovskikh and Boehler 2001; Zhang and Smyth 2022). The olivine polymorphs can also be the major nickel reservoirs in the mantle (Ishimaru and Arai 2008; Straub et al. 2008; Zhang et al. 2018; Demouchy and Alard 2021; Zhang and Smyth 2022). In some localities such as Barberton, South Africa and Lavrion, Greece, Ni-dominant olivine (liebenbergite) and Ni-rich olivine do occur naturally (De Waal and Calk 1973; Tredoux et al. 1989; Koshlyakova et al. 2017). According to previous experimental investigations, pure liebenbergite transforms to Ni_2SiO_4 spinel at only 2–3 GPa (dependent on temperature) (Akimoto et al. 1965; Ma 1974). Therefore, the high-pressure and high-temperature behaviors of olivine polymorphs in Ni_2SiO_4 are expected to be significantly different from those in $(Mg, Fe)_2SiO_4$.

The crystal structure of liebenbergite consists of two symmetrically distinct NiO_6 octahedral sites (M1 and M2) and one isolated SiO_4 tetrahedral site (Si site). It is orthorhombic

✉ Li Zhang
li.z.zhang@cugb.edu.cn

1 School of Earth Sciences and Resources, China University of Geosciences, Beijing 100083, China

2 Center for High Pressure Science and Technology Advanced Research, Beijing 100193, China

3 State Key Laboratory of Lithospheric Evolution, Institute of Geology and Geophysics, Chinese Academy of Sciences, Beijing 100029, China

4 Institute of Geology, Chinese Academy of Geological Sciences, Beijing 100037, China

in the *Pbnm* space group. By contrast, Ni_2SiO_4 spinel is cubic in the $Fd\bar{3}m$ space group and contains only one octahedral site and one isolated tetrahedral site (Finger et al. 1979; Gartvich and Galkin 2019). The unit-cell parameters and crystal structures of Ni_2SiO_4 liebenbergite and spinel were previously measured at various pressure and temperature by the X-ray diffraction method (Mao et al. 1970; Sato 1977; Finger et al. 1979; Gartvich and Galkin 2019; Zhang et al. 2019). Based on the measurements under compression up to 12 and 30 GPa, the values K_T (isothermal bulk modulus) of Ni_2SiO_4 spinel were calculated to be 214 and 223 GPa, respectively (Mao et al. 1970; Sato 1977). Finger et al. (1979) showed that, for Ni_2SiO_4 spinel, the polyhedral bulk modulus is about 170 GPa for the NiO_6 octahedron and is greater than 250 GPa for the SiO_4 tetrahedron. Zhang et al. (2019) found that liebenbergite can be the most incompressible olivine-group silicate. On the basis of the compressional equation of state measurement up to 42.6 GPa at room temperature, the value K_T of liebenbergite was estimated to be about 163 GPa. Gartvich and Galkin (2019) determined temperature dependencies of molar volumes and coefficients of bulk thermal expansion of liebenbergite, and showed that the values of adiabatic bulk modulus K_S and isothermal bulk modulus K_T can be about 165 GPa and 163.7 GPa, respectively. For both Ni_2SiO_4 spinel and liebenbergite, according to Finger et al. (1979), the ratio of Ni-O distance in the octahedral site to Si-O distance in the tetrahedral site, (d_o/d_t), decreases with increasing pressure or decreasing temperature.

Yamanaka and Ishii (1986) measured Raman spectra of Ni_2SiO_4 spinel in the temperature range of 20–600 °C, and suggested that the Si-O bond can be significantly weakened at high temperatures. Lin (2001a) studied the Raman spectra of synthetic liebenbergite under compression up to 35 GPa in the quasi-hydrostatic (water was used as the pressure medium) and non-hydrostatic (no pressure medium) pressure environments. The results indicate that the distortion of SiO_4 tetrahedra may be more severe than that of NiO_6 octahedra at high pressures.

To better understand the high-pressure and high-temperature behaviors of liebenbergite and Ni_2SiO_4 spinel and the effects of nickel on the vibration properties of olivine and spinel-group minerals, we have synthesized liebenbergite and Ni_2SiO_4 spinel at 5 GPa, 1420 °C and 5 GPa, 1500 °C, respectively. Tescan integrated mineral analyzer (TIMA) and single-crystal X-ray diffractometer were used to investigate their chemical compositions and crystal structures. *In-situ* high-pressure (argon was used as the pressure medium) and high-temperature Raman spectroscopic measurements of liebenbergite and Ni_2SiO_4 spinel have been conducted up to 22 GPa and 700 °C, respectively. Isothermal and isobaric mode Grüneisen parameters were calculated based on the experimental data. In addition, the intrinsic anharmonicities of liebenbergite and Ni_2SiO_4 spinel were also evaluated.

Experimental work

The liebenbergite and Ni_2SiO_4 spinel samples were respectively synthesized at 5 GPa, 1500 °C and 5 GPa, 1420 °C with heating time of 8 h in the GY-420 cubic-anvil apparatus at Center for High Pressure Science and Technology Advanced Research, Beijing. Pressure was calibrated based on Bi I-II and quartz-coesite phase transition at 2.55 GPa, room temperature and 3.2 GPa, 1100 °C, respectively. The temperature effect during the calibration process was not considered. High-purity oxide powders (NiO and SiO_2) were mixed using ethanol in an agate mortar for 1–2 h and dried at 110 °C overnight. The mixed starting material powder was then filled into a Pt capsule (ID 3.2 mm, OD 3.5 mm, length 5 mm). To minimize thermal gradient, the capsule was put at the center of a graphite heater. During the experiments, the starting materials were cold pressed to target pressure and then heated to target temperature with a rate of 100 °C/min. Temperature was monitored using a W3Re-W25Re (type D) thermocouple controller. The runs were quenched by cutting the power and temperature (typically dropped down to 100 °C in <50 s). The recovered capsules were mounted in epoxy and polished to expose the polycrystalline specimens.

For phase identification, the polished capsules were scanned by a TIMA3X FEG LMH analyzer with 8.83 nA probe current and 25,000 eV beam energy. The working distance, spot size, and pixel size were 15 mm, 91.67 nm, and 1 μm, respectively. The representative SEM images of the exposed run products are shown in Fig. 1. For crystal structure analysis, single crystals of liebenbergite and Ni_2SiO_4 spinel were selected from the run products, and then analyzed by using a Bruker D8 Venture X-ray diffractometer with a PHOTON detector. The X-ray ($\lambda = 0.71073$ Å) was generated at 50 kV and 1.4 mA via a IμS 3.0 generator equipped with a Mo anode. The crystal structures were refined from the collected intensity data with SHELX (Sheldrick 2015) in WINGX software (Farrugia 2012). The refinements were based on the reported scattering factors and absorption coefficients for Ni, O and Si in International Tables for Crystallography, Volume C (Prince 2004). The unit-cell and atom position parameters (Table S1) are estimated based on the results of single-crystal X-ray diffraction analyses. The X-ray powder diffraction patterns for Cu Kα radiation ($\lambda = 1.5405$ Å) of liebenbergite and Ni_2SiO_4 spinel were calculated using Vesta software (Fig. S1). As shown in Fig. 1, most of the starting composition successfully transformed to liebenbergite and Ni_2SiO_4 spinel, while

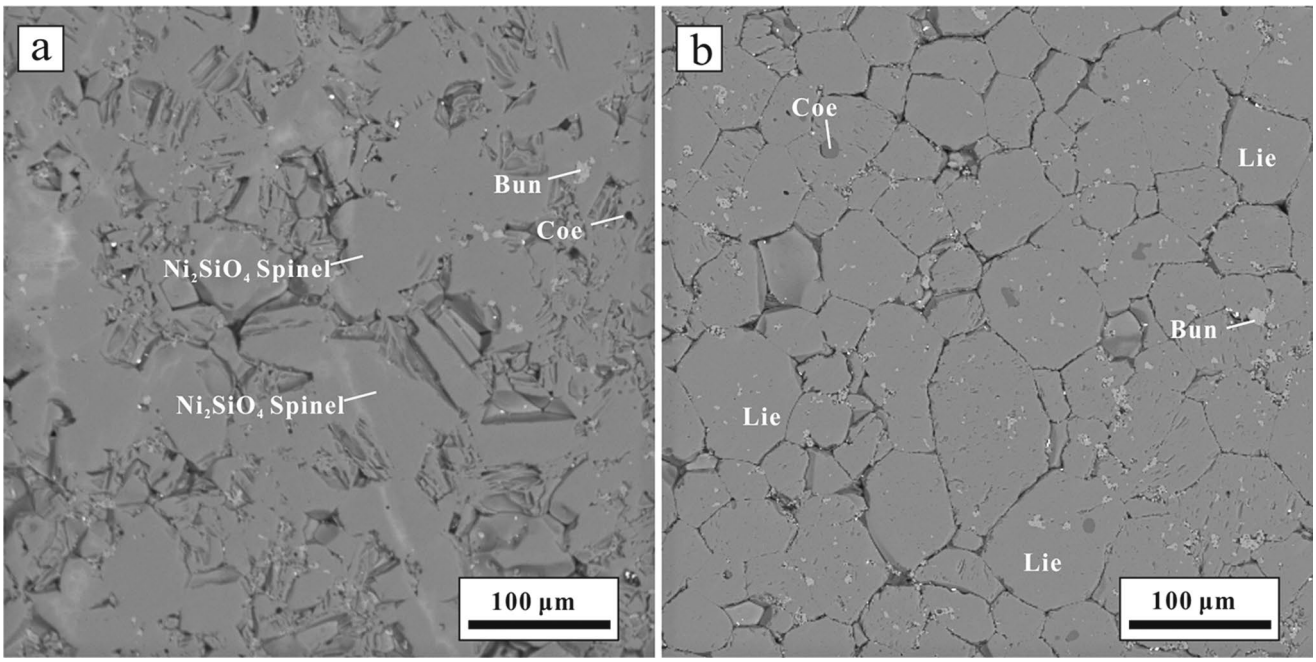

Fig. 1 SEM (Scanning Electron Microscope) images of high-pressure and high-temperature experimental products. **(a)** at 5 GPa, 1420 °C and **(b)** at 5 GPa, 1500 °C. *Lie* liebenbergite, *Bun* bunsenite, and *Coe* coesite

minor residual unreacted NiO and SiO_2 remain as bunsenite and coesite.

In the high-pressure Raman spectroscopic measurements, a pair of type Ia diamond anvils with 300 μm culet diameter was used to compress the sample in a symmetric-type diamond-anvil cell (DAC). The unoriented chips of liebenbergite (about 50 × 50 × 30 μm in size) and Ni_2SiO_4 spinel (about 40 × 30 × 30 μm in size) were loaded separately into the hole (approximately 150 μm in diameter and 40–50 μm in depth) in a rhenium gasket with one or two ruby spheres. Argon (Ar) was used as the pressure-transmitting medium. According to Klotz et al. (2009), the potential pressure gradients are expected to be lower than 0.2 GPa at pressures up to 20 GPa. Due to the rapid increase in pressure gradients over 20 GPa, the spectra obtained below 20 GPa were used to analyze the variations in Raman modes under compression and decompression. Raman spectra were collected by a HORIBA LabRAM HR Evolution laser Raman spectrometer with a 20×microscope objective at Institute of Geology, Chinese Academy of Geological Sciences. All spectra were excited by a 532 nm solid-state laser and collected in the wavenumber range from 100 to 1200 cm^{-1}, using 10 accumulations and 5 s exposure time with a spectral resolution of 1 cm^{-1}. A laser power of 40 mW was used at the surface of the sample. Pressures were estimated based on the shift of the ruby R1 luminescent line (Chijioke et al. 2005).

Raman spectra of the unoriented liebenbergite (about 50 × 40 × 40 μm in size) and Ni_2SiO_4 spinel (about 40 × 30 × 30 μm in size) at various temperature were analyzed by a WITec's confocal Raman imaging microscope alpha300 R with a 20 × objective at Institute of Geology and Geophysics, Chinese Academy of Sciences. A Linkam TS1400 heating stage with a SiO_2 window and a Rh/Pt thermocouple was used for the high-temperature measurements at 25, 100, 200, 300, 400, 500, 600, and 700 °C during heating and cooling (increasing and decreasing rates are 50 °C/min and − 50 °C/min, respectively). At each temperature, the sample was held for 10 min to reach equilibrium. All spectra were excited by a 488-nm solid-state laser and collected in the wavenumber range of 200–1000 cm^{-1} with 40 mW power on the sample, using 1800 gr/mm grating with 15 accumulations and 20 s exposure time.

Results and discussion

Raman spectra of liebenbergite and Ni_2SiO_4 spinel at ambient conditions

As summarized in Fig. 2, the unpolarized Raman spectrum of liebenbergite displays 15 bands at 221, 254, 272, 294, 300, 305, 347, 425, 560, 567, 819, 840, 867, 890, and 954 cm^{-1} at ambient conditions. All these bands are in agreement with those observed in previous studies (Lin 2001a, b). The bands at 221, 254, 294, 300, and 305 cm^{-1} are assigned to the M2 and SiO_4 translations (A_g). The bands at 272 (B_{2g}) and 347 cm^{-1} (B_{3g}) are due to SiO_4 rotations. The 425 cm^{-1} band and the two bands at about 560 cm^{-1} correspond to the

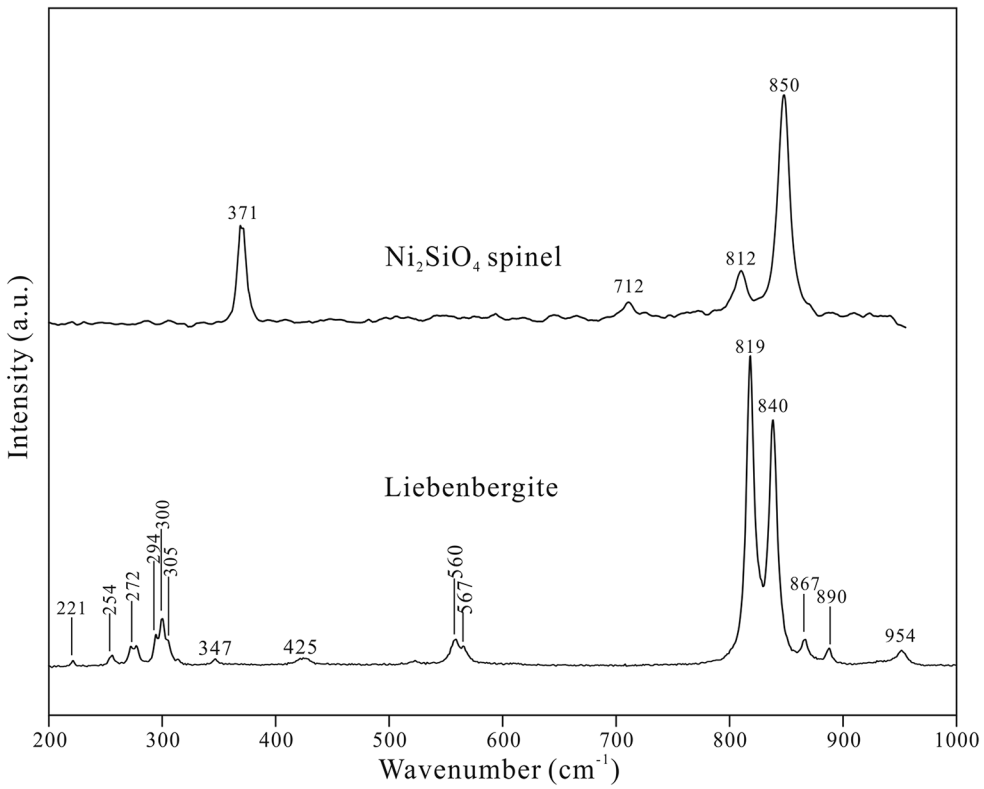

Fig. 2 Raman spectra of liebenbergite and Ni_2SiO_4 spinel at ambient conditions in the wavenumber range of 200–1000 cm^{-1}

symmetric (v_2) and asymmetric (v_4) deformation of the SiO_4 tetrahedron, respectively. The last four bands (at 840, 867, 890, and 954 cm^{-1}) and the intense band at 819 cm^{-1} are assigned to the asymmetric (v_3) and symmetric (v_1) stretching of the SiO_4, respectively (Lin 2001a, b).

Under ambient conditions, the unpolarized Raman spectrum of Ni_2SiO_4 spinel contains three strong bands at 371, 812 and 850 cm^{-1} (Fig. 2). The latter two bands at 812 and 850 cm^{-1} are assigned to the asymmetric (T_{2g}) and symmetric (A_{1g}) stretching of the SiO_4 tetrahedron, respectively (Chopelas et al. 1994; Kleppe et al. 2002b), while the band at 371 cm^{-1} corresponds to the deformation (E_g) of the SiO_4. The weak band at 712 cm^{-1} is typically assigned to the SiO_4 internal vibrations in crystal structures of olivine and spinel-group minerals (Yamanaka and Ishii 1986; Chopelas et al. 1994; Yang et al. 2015; Liu et al. 2021). In hydrous Mg-Fe ringwoodite, according to Kleppe et al. (2002a), this band can be due to stretching of Si_2O_7 dimer, which is incompatible with the ideal spinel structure (contains only isolated SiO_4 tetrahedra). The presence of the dimer with a bridging oxygen in the spinel structure, would require a non-silicate oxygen elsewhere which could act as site for protonation (Kleppe et al. 2002a). Therefore, Si_2O_7 groups are not expected to exist in the crystal structure of the anhydrous Ni_2SiO_4 spinel in this study.

Raman spectra of liebenbergite and Ni_2SiO_4 spinel as a function of pressure

The representative Raman spectra of liebenbergite and Ni_2SiO_4 spinel as a function of increasing and decreasing pressure are shown in Figs. 3 and 4, respectively. For liebenbergite, the three bands (at 560, 819, and 840 cm^{-1} under ambient pressure) caused by the stretching and deformation of the SiO_4 shift continuously to higher frequencies with increasing pressure up to 22.54 GPa. As shown in Fig. 5, these spectral changes are reversible on decompression. The intensities of the other eight bands observed at ambient conditions decrease progressively during compression. As a result, these bands gradually become indistinguishable in the pressure range of 1.36–15.98 GPa. However, they recover in the identical range with decreasing pressure (Table S2). In addition, no new modes can be observed in all the spectra during compression and decompression (Fig. 3). Thus, liebenbergite is not expected to undergo remarkable changes in crystal structure within the studied pressure range.

For Ni_2SiO_4 spinel, the three bands associated with the stretching and deformation of the SiO_4 shift continuously up to 21.70 GPa under compression. The weak band at 712 cm^{-1} is difficult to be observed due to its low intensity (Fig. 4). The two intense SiO_4 stretching bands (at 812 and 850 cm^{-1} under ambient pressure) of Ni_2SiO_4 spinel shift

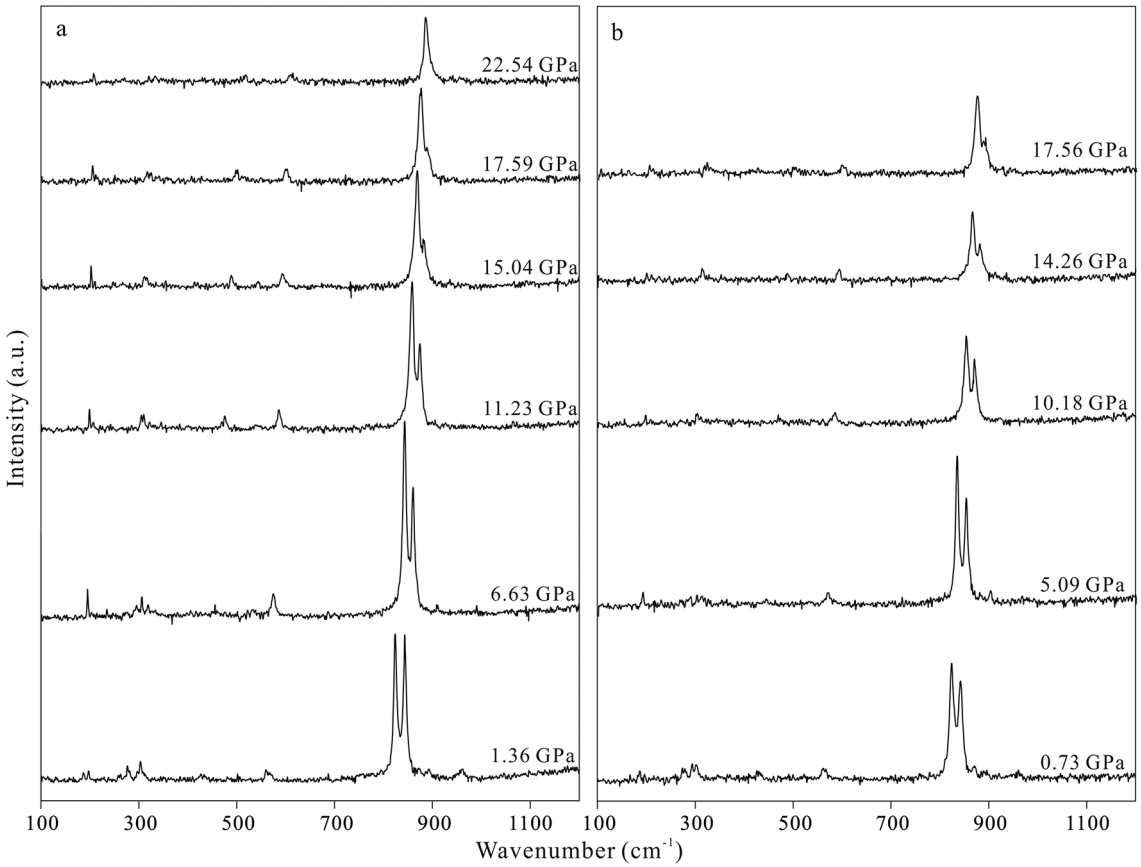

Fig. 3 Representative Raman spectra of liebenbergite with varying pressure under **(a)** compression and **(b)** decompression

faster in frequency with increasing pressure than those (at 819 and 840 cm^{-1} under ambient pressure) of liebenbergite (3.20–3.39 cm^{-1}/GPa compared to 3.03–3.14 cm^{-1}/GPa) (Table 1). The frequencies of the asymmetric SiO_4 stretching band (at 812 cm^{-1} under ambient pressure) can be strongly affected by the unit-cell parameters and increase nearly linearly with decreasing cell volume (Chopelas et al. 1994). As presented in Fig. 5 and Table S3, the frequency changes of this band are irreversible under decompression, indicating a pressure-induced modification in the crystal structure. According to Kamb (1968), the stability limit of Ni_2SiO_4 spinel can be simply defined by the ratio (d_o/d_t) of octahedral (Ni-O) to tetrahedral (Si-O) distance. During compression, the d_o/d_t ratio decreases with decreasing cell volume (Finger et al. 1979). Meanwhile, the stability of the crystal structure can be reinforced (Kamb 1968). Therefore, the modification may easily be retained under decompression. *In-situ* high-pressure X-ray diffraction investigations (on compression and decompression) are expected to further explain the irreversible frequency changes observed in this study.

Raman spectra of liebenbergite and Ni_2SiO_4 spinel as a function of temperature

The Raman spectra of liebenbergite and Ni_2SiO_4 spinel as a function of increasing and decreasing temperature in the range of 25–700 °C are shown in Figs. 6 and 7, respectively. For liebenbergite, the bands observed at ambient temperature shift continuously to lower frequencies with increasing temperature up to 700 °C (Figs. 6 and 8). In all the spectra collected during heating and cooling, no new bands and no evidence for temperature-induced amorphization can be observed. As shown in Fig. 8 and Table S4, all the bands return to their initial frequencies at ambient temperature after cooling, indicating no irreversible modifications of the crystal structure within the studied temperature range.

The Raman bands of Ni_2SiO_4 spinel also exhibit shifts to lower wavenumber upon heating to 700 °C (Figs. 7 and 8). The vibrational bands of the SiO_4 (at 371, 812, 850 cm^{-1} under ambient temperature) and their shifts are similar to those reported in the previous high-temperature (up to 600 °C) Raman study (Yamanaka and Ishii 1986). As shown in Fig. 8 and Table S5, the frequencies of the bands are fully reversible upon cooling. In addition, no bands disappear and

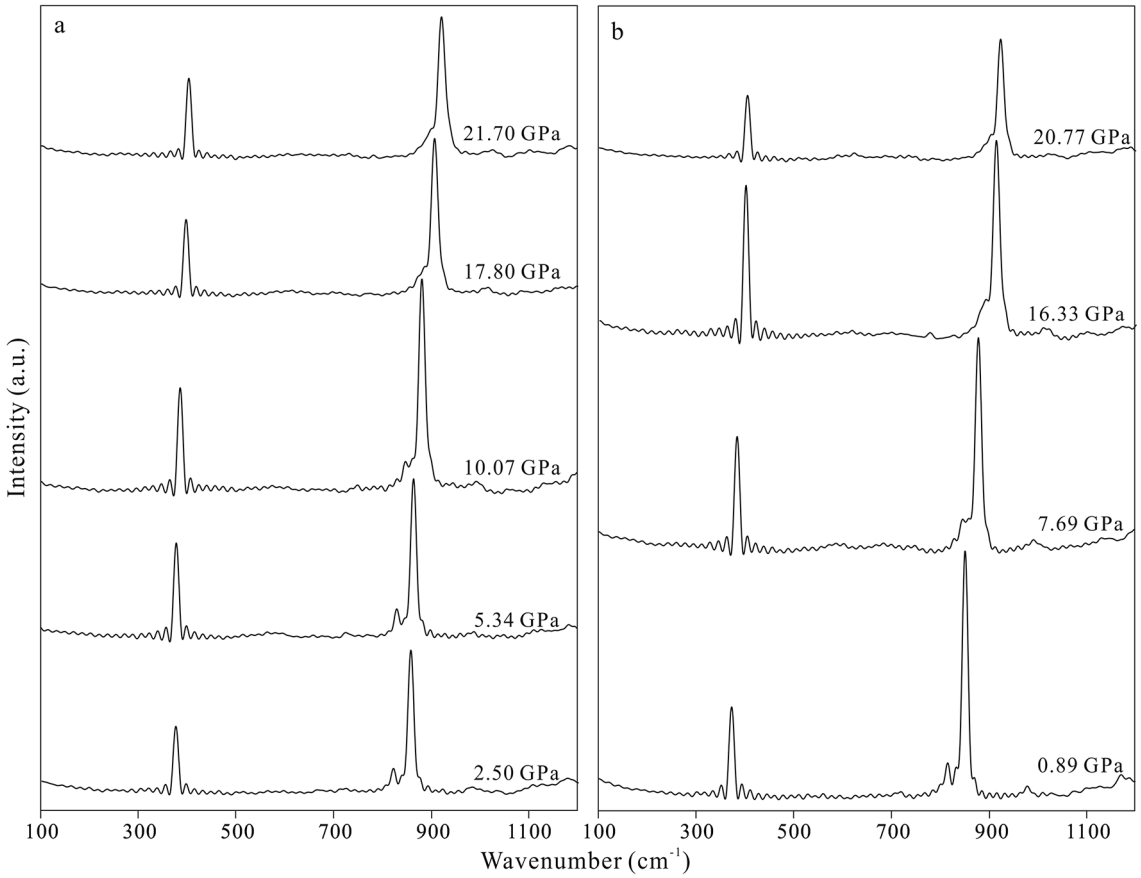

Fig. 4 Representative Raman spectra of Ni_2SiO_4 spinel with varying pressure under **(a)** compression and **(b)** decompression

no new bands emerge during heating and cooling. These results show no remarkable modifications of the Ni_2SiO_4 spinel sample in the investigated temperature range. During heating, the d_o/d_t ratio increases with increasing cell volume (Finger et al. 1979), resulting in a reduced stability of the crystal structure (Kamb 1968). Thus, the potential modification can hardly be retained upon cooling.

As shown in Table 1, the strong band (at 850 cm^{-1} under ambient temperature) associated with the symmetric SiO_4 stretching of Ni_2SiO_4 spinel shifts slower in frequency than that (at 840 cm^{-1} under ambient temperature) of liebenbergite upon heating (-0.014 cm^{-1}/°C compared to -0.018 cm^{-1}/°C). In contrast, the asymmetric stretching band of the SiO_4 (at 812 cm^{-1} under ambient temperature) of Ni_2SiO_4 spinel shifts significantly faster than that (at 819 cm^{-1} under ambient temperature) of liebenbergite (-0.034 cm^{-1}/°C compared to -0.006 cm^{-1}/°C). Based on the previous investigation (Chopelas et al. 1994), the unit cell of Ni_2SiO_4 spinel is therefore believed to vary more rapidly in size with temperature.

Grüneisen parameters and anharmonicity

The isothermal mode Grüneisen parameter γ_{iT} and the isobaric mode Grüneisen parameter γ_{iP} represent the pressure and temperature dependence of the *i*th vibration mode at a constant temperature and constant pressure, respectively (Yang et al. 2017; Zhai et al. 2020).

The isothermal mode Grüneisen parameter γ_{iT} is calculated using the equation:

$$\gamma_{iT} = \frac{K_T}{v_i}\left(\frac{\partial v_i}{\partial P}\right)_T \quad (1)$$

The isobaric mode Grüneisen parameter γ_{iP} is calculated using the equation:

$$\gamma_{iP} = \frac{1}{\alpha v_i}\left(\frac{\partial v_i}{\partial T}\right)_P \quad (2)$$

Where v_i is the Raman band of the *i*th vibrational mode at ambient temperature, $\left(\frac{\partial v_i}{\partial P}\right)_T$ and $\left(\frac{\partial v_i}{\partial T}\right)_P$ are the temperature and pressure derivatives of the Raman frequency obtained from the compression and heating processes in this

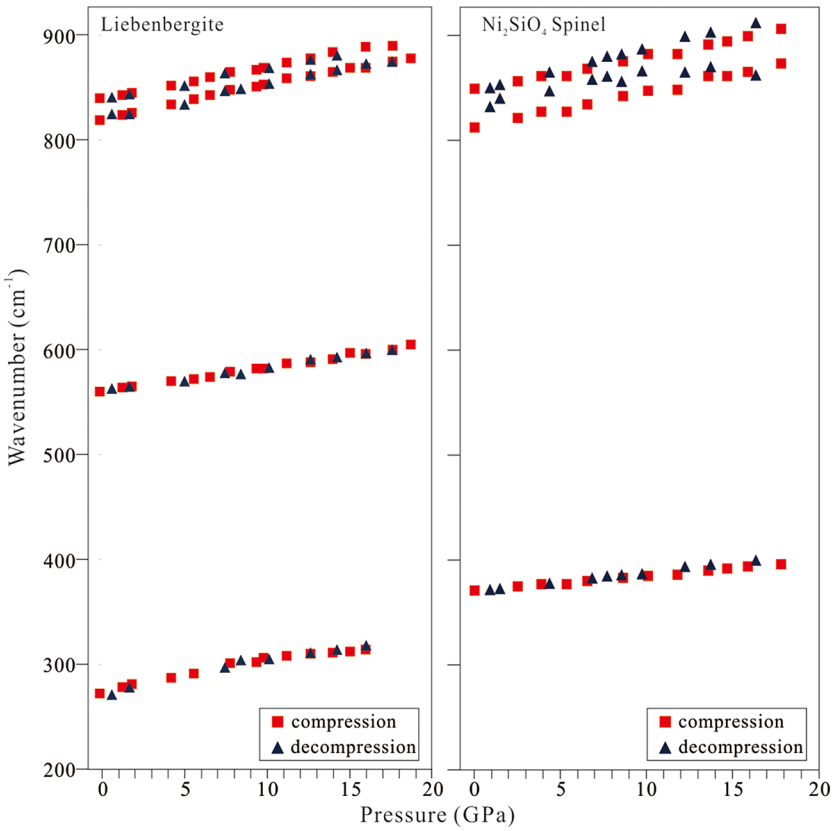

Fig. 5 Pressure dependence of the vibrational modes for liebenbergite and Ni_2SiO_4 spinel at ambient temperature. Errors are within the size of the symbols

Table 1 Frequencies of Raman modes, corresponding temperature/pressure derivatives, isothermal mode Grüneisen parameter γ_{iT}, isobaric mode Grüneisen parameter γ_{iP}, intrinsic anharmonic mode parameter a_i, and assignment

	ν_i at ambient condition (cm^{-1})	(cm^{-1}/°C)	γ_{iP}	(cm^{-1}/GPa)	γ_{iT}	a_i ($10^{-5}K^{-1}$)	Assignments	References
Ni_2SiO_4 Spinel	371(1)	-0.022(1)	2.20(5)	1.41(4)	0.86(3)	-3.63(1)	SiO_4 deformation	[1][2]
	812(1)	-0.034(2)	1.56(6)	3.39(11)	0.94(3)	-1.66(1)	asymmetric SiO_4 stretching	[2][3]
	850(1)	-0.014(1)	0.61(7)	3.20(10)	0.85(3)	0.64(1)	symmetric SiO_4 stretching	[2][3]
Liebenbergite	272(2)	-0.011(2)	1.47(26)	2.62(16)	1.57(6)	0.29(7)	M2 translation; SiO_4 rotation	[4][5]
	300(1)	-0.021(1)	2.54(5)	–	–	–	M2 translation; SiO_4 rotation	[4][5]
	560(1)	-0.013(4)	0.84(31)	2.32(5)	0.68(2)	-0.46(7)	asymmetric SiO_4 deformation	[4]
	819(1)	-0.006(2)	0.27(33)	3.14(7)	0.62(2)	0.99(1)	symmetric SiO_4 stretching	[4]
	840(1)	-0.018(1)	0.78(6)	3.03(6)	0.59(2)	-0.52(1)	asymmetric SiO_4 stretching	[4]
	868(2)	-0.023(4)	0.96(17)	–	–	–	asymmetric SiO_4 stretching	[4]
	890(5)	-0.027(5)	1.10(19)	–	–	–	asymmetric SiO_4 stretching	[4]
	954(1)	-0.017(3)	0.65(18)	–	–	–	asymmetric SiO_4 stretching	[4]

[1] Yamanaka and Ishii (1986); [2] Chopelas et al. (1994); [3] Kleppe et al. (2002a); [4] Lin (2001a); [5] McKeown et al. (2010)

study, K_T is the isothermal bulk modulus at ambient temperature and α is thermal expansion coefficient.

The isothermal bulk modulus $K_T = 163$ GPa for liebenbergite (Zhang et al. 2019) and $K_T = 226$ GPa for Ni_2SiO_4 spinel (Bass et al. 1984) were used in the γ_{iT} calculation. To simplify the calculation (Liu et al. 2019), the average volume thermal expansion coefficients of 2.76×10^{-5} K^{-1} for liebenbergite (Kroll et al. 2019), 2.69×10^{-5} K^{-1} for Ni_2SiO_4 spinel (Finger et al. 1979) and 3.08×10^{-5} K^{-1} for ringwoodite (Katsura et al. 2004) were used in the γ_{iP} calculation.

As presented in Table 1; Figs. 9 and 10, the lattice vibration modes have higher γ_{iT} and γ_{iP} values than the SiO_4 internal vibration modes in the crystal structures of both liebenbergite and forsterite. This indicates that the lattice vibrations are generally more sensitive to the variations of pressure and temperature compared to the SiO_4 internal vibrations in olivines that contain metal cations with different radii.

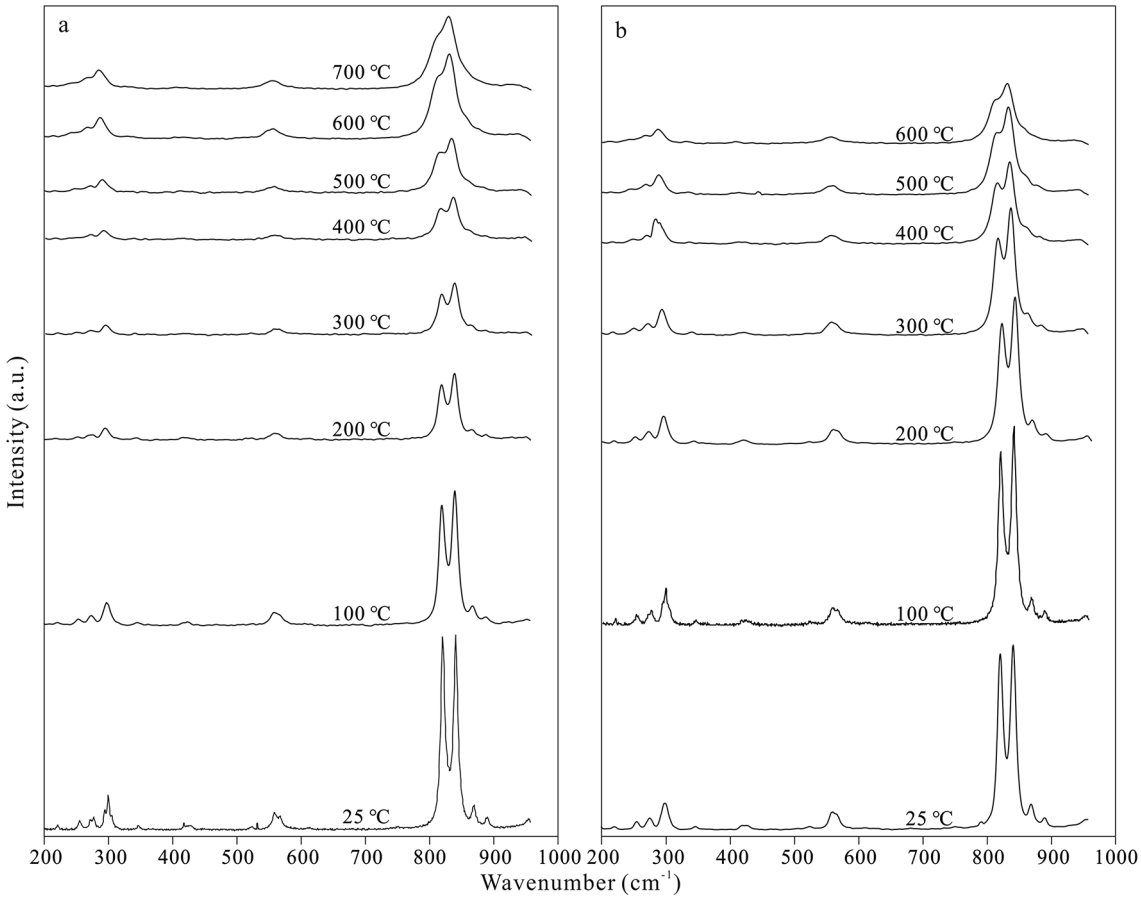

Fig. 6 Raman spectra of liebenbergite with varying temperature upon **(a)** heating and **(b)** cooling

The SiO_4 internal vibration modes (at 560, 819 and 840 cm^{-1}) of liebenbergite have higher γ_{iT} values than those of forsterite. However, the SiO_4 internal vibration modes (at 812 and 850 cm^{-1}) of Ni_2SiO_4 spinel have lower γ_{iT} values than those of ringwoodite (Table 1; Fig. 9). Therefore, nickel in olivine structure is believed to increase the sensitivity of the SiO_4 internal vibrations to the variations of pressure. By comparison, these vibrations in spinel structure can be less sensitive to the pressure change due to nickel incorporation. As shown in Table 1; Fig. 10, the γ_{iP} values of the SiO_4 internal vibration modes for Ni_2SiO_4 spinel are significantly higher than those for ringwoodite, revealing that nickel in the spinel structure increases the sensitivity of these vibrations to the variations of temperature.

The intrinsic anharmonic mode parameter a_i is calculated based on the following equation:

$$a_i = -\alpha\left(\gamma_{iP} - \gamma_{iT}\right) \tag{3}$$

The non-zero a_i values (Table 1; Fig. 11) indicate that intrinsic anharmonicity exists in both liebenbergite and Ni_2SiO_4 spinel. According to Gillet et al. (1991), the a_i values are negative for all vibration modes in forsterite (Fig. 11). However, in liebenbergite, the a_i values for the lattice vibration mode at 272 cm^{-1} and the SiO_4 internal vibration mode at 819 cm^{-1} are positive, though the values for the modes at 560 and 840 cm^{-1} are also negative (Fig. 11). In ringwoodite, the a_i values for the SiO_4 internal vibration modes are positive. Whereas, the value for the asymmetric SiO_4 stretching mode (at 812 cm^{-1}) in Ni_2SiO_4 spinel is negative, though the value for the symmetric SiO_4 stretching mode (at 850 cm^{-1}) is also positive. These imply that nickel in olivine and spinel structures has distinctive effects on the intrinsic anharmonicities of different vibration modes.

Nickel is the fifth most abundant element in the Earth. The estimated concentrations of this element in the core, mantle, and bulk Earth are respectively 5.2 wt%, 0.2 wt%, and 1.82 wt% (McDonough 2014). However, the estimation of nickel concentration in the mantle is based heavily on the chemical compositions of rocks in the shallow upper mantle (Matzen et al. 2013; McDonough 2014; Palme and O'Neill 2014). The minerals in these rocks are too far removed from their mantle source to provide information on the enrichment of nickel in the interior of the silicate Earth (Matzen et al. 2013; Pu et al. 2017; Putirka et al. 2018). It is possible that nickel can be enriched in the olivine polymorphs in the

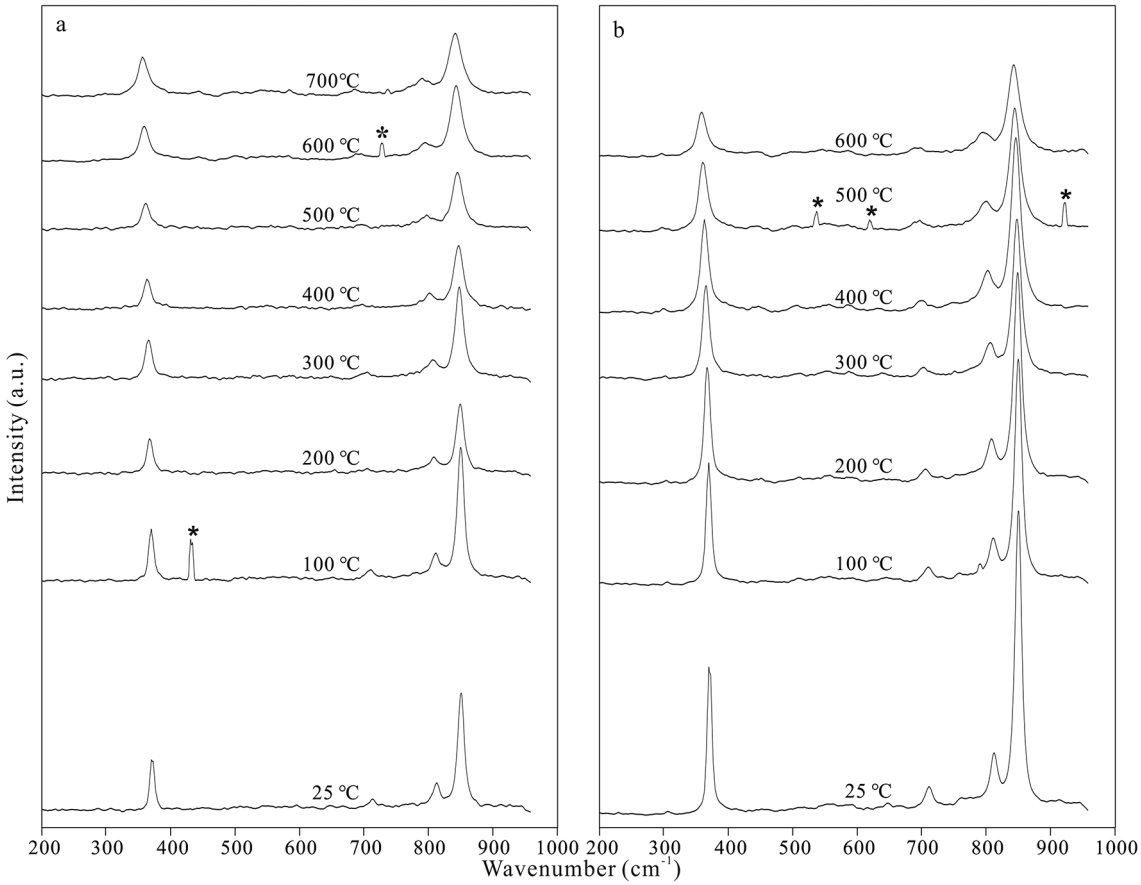

Fig. 7 Raman spectra of Ni_2SiO_4 spinel with varying temperature upon **(a)** heating **(b)** cooling. The asterisk represents the signal from cosmic rays

deep part of the mantle under specific geological settings (Matzen et al. 2013; Zhang et al. 2019; Zhang and Smyth 2022). This study indicates that Ni incorporation can influence the thermodynamic properties of olivine and spinel group minerals by altering Grüneisen parameters of vibration modes and intrinsic anharmonicities. Since the mode Grüneisen parameters were calculated only based on Raman active optical phonons in the present work, more experimental and theoretical investigations are required to further reveal the Grüneisen parameters of phonon modes across the entire Brillouin zone.

Conclusions

(1) For Ni_2SiO_4 spinel, the changes of the asymmetric SiO_4 stretching band in frequency are irreversible during decompression, indicating a potential pressure-induced modification in the crystal structure at elevated pressures up to 22 GPa.
(2) Nickel in olivine structure increases the sensitivity of the SiO_4 internal vibrations to the variations of pressure. Due to nickel incorporation, the SiO_4 internal vibrations in spinel structure can be less sensitive to the pressure change. However, these vibrations are more sensitive to the variations of temperature.
(3) Nickel has distinctive effects on the intrinsic anharmonicity of different vibration modes in olivine and spinel structures.

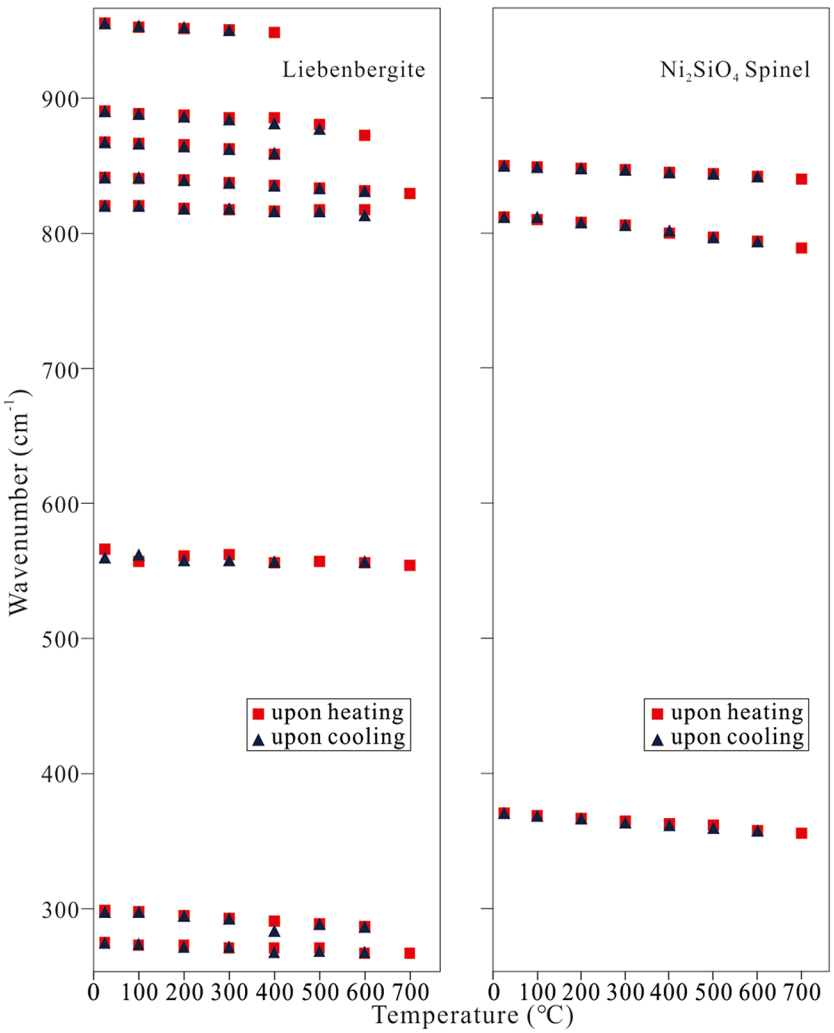

Fig. 8 Temperature dependence of the vibrational modes for liebenbergite and Ni_2SiO_4 spinel at ambient pressure. Errors are within the size of the symbols

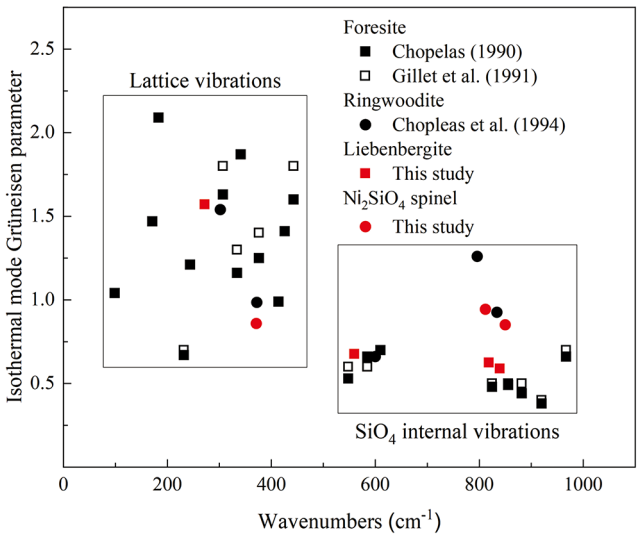

Fig. 9 Isothermal mode Grüneisen parameters for various Raman mode frequencies in forsterite (Chopelas 1990; Gillet et al. 1991), ringwoodite (Chopelas et al. 1994), liebenbergite and Ni_2SiO_4 spinel

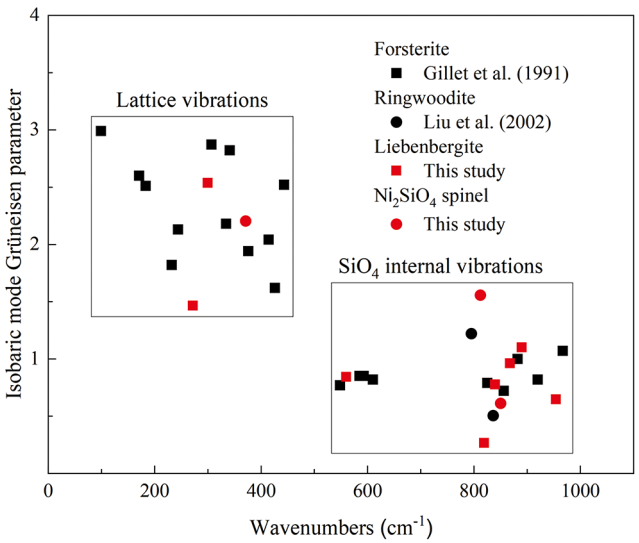

Fig. 10 Isobaric mode Grüneisen parameters for various Raman mode frequencies in forsterite (Gillet et al. 1991), ringwoodite, liebenbergite and Ni_2SiO_4 spinel. The isobaric mode Grüneisen parameter of ringwoodite was recalculated based on the temperature dependence reported in Liu and Mernagh (1994) and Liu et al. (2002)

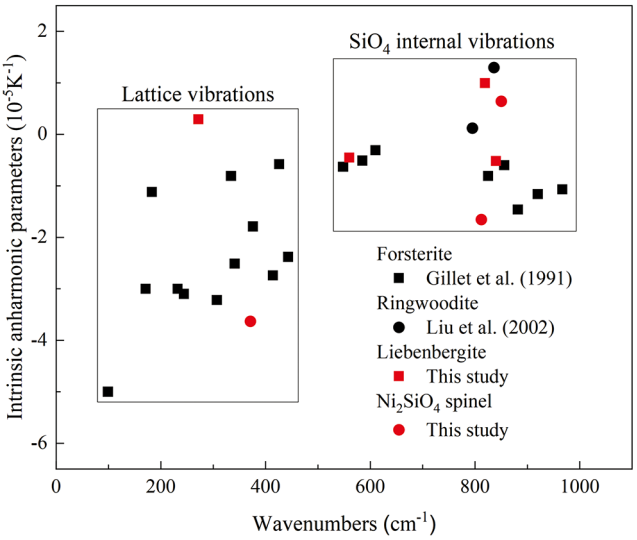

Fig. 11 Intrinsic anharmonic parameters for various Raman mode frequencies in forsterite (Gillet et al. 1991), ringwoodite (Liu et al. 2002), liebenbergite and Ni_2SiO_4 spinel

Supplementary Information The online version contains supplementary material available at https://doi.org/10.1007/s00269-024-01295-4.

Author contributions L.Z. suggested the basis of the paper; L.Z. and S.G. wrote the main manuscript text; S.G. and H.C. performed high-pressure and high-temperature experiments; J.L. performed TIMA analysis; S.G. and X.L. performed high-temperature Raman measurements; S.G, J.L., and X.Q. performed high-pressure Raman measurements. L.Z. and Y.L. suggested and discussed the methods and results; All authors reviewed the manuscript.

Funding This study was supported by the National Natural Science Foundation of China (No. 42172044 to L.Z. and 42250105 to Y.L.) and the Fundamental Research Funds for the Central Universities.

Data availability Data is provided within the manuscript or supplementary information files.

Declarations

Conflict of interest The authors declare that they have no conflict of interest.

References

Akimoto SI, Fujisawa H, Katsura T (1965) The olivine-spinel transition in Fe_2SiO_4 and Ni_2SiO_4. J Geophys Res 70(8):1969–1977. https://doi.org/10.1029/JZ070i008p01969

Bass JD, Weidner DJ, Hamaya N, Ozima M, Akimoto S (1984) Elasticity of the olivine and spinel polymorphs of Ni_2SiO_4. Phys Chem Min 10:261–272. https://doi.org/10.1007/BF00311951

Chijioke AJ, Nellis WJ, Soldatov A, Silvera IF (2005) The ruby pressure standard to 150 GPa. J Appl Phys 98(11):114905. https://doi.org/10.1063/1.2135877

Chopelas A (1990) Thermal properties of forsterite at mantle pressures derived from vibrational spectroscopy. Phys Chem Min 17:149–156. https://doi.org/10.1007/BF00199666

Chopelas A, Boehler R, Ko T (1994) Thermodynamics and behavior of γ-Mg_2SiO_4 at high pressure: implications for Mg_2SiO_4 phase equilibrium. Phys Chem Min 21:351–359. https://doi.org/10.1029/GL010i001p00087

Chudinovskikh L, Boehler R (2001) High-pressure polymorphs of olivine and the 660-km seismic discontinuity. Nature 411:574–577. https://doi.org/10.1038/35079060

De Waal SA, Calk LC (1973) Nickel minerals from Barberton, South Africa: VI. Liebenbergite, a nickel olivine. Am Min 58(7–8):733–735

Demouchy S, Alard O (2021) Hydrogen, trace, and ultra-trace element distribution in natural olivines. Phys Chem Min 176:26. https://doi.org/10.1007/s00410-021-01778-5

Farrugia LJ (2012) WinGX and ORTEP for Windows: an update. J Appl Crystallogr 45(4):849–854. https://doi.org/10.1107/S0021889812029111

Finger LW, Hazen RM, Yagi T (1979) Crystal structures and electron densities of nickel and iron silicate spinels at elevated temperature or pressure. Am Min 64(9–10):1002–1009

Gartvich Y, Galkin V (2019) Ni olivine: thermal behavior of liebenbergite. J Therm Anal Calorim 136:2333–2339. https://doi.org/10.1007/s10973-018-7859-6

Gillet P, Richet P, Guyot F, Fiquet G (1991) High-temperature thermodynamic properties of forsterite. J Geophys Res 96(B7):11805–11816. https://doi.org/10.1029/91JB00680

Ishimaru S, Arai S (2008) Nickel enrichment in mantle olivine beneath a volcanic front. Contrib Mineral Petr 156:119–131. https://doi.org/10.1007/s00410-007-0277-6

Kamb B (1968) Structural basis of the olivine-spinel stability relation. Am Min 53(9–10):1439–1455

Katsura T, Yokoshi S, Song M, Kawabe K, Tsujimura T, Kubo A, Ito E, Tange Y, Tomioka N, Saito K, Nozawa A, Funakoshi K (2004) Thermal expansion of Mg_2SiO_4 ringwoodite at high pressures. J Geophys Res 109:B12209. https://doi.org/10.1029/2004JB003094

Kleppe AK, Jephcoat AP, Smyth JR (2002a) Raman spectroscopic study of hydrous γ-Mg_2SiO_4 to 56.5 GPa. Phys Chem Min 29:473–476

Kleppe AK, Jephcoat AP, Smyth JR, Frost DJ (2002b) On protons, iron and the high-pressure behavior of ringwoodite. Geophys Res Lett 29(21):17. https://doi.org/10.1029/2002GL015276. -1-17-4

Klotz S, Chervin JC, Munsch P, Le Marchand G (2009) Hydrostatic limits of 11 pressure transmitting media. J Phys D: Appl Phys 42(7):075413. http://iopscience.iop.org/0022-3727/42/7/075413

Kohlstedt DL, Keppler H, Rubie DC (1996) Solubility of water in the α, β, and γ phases of $(mg,Fe)_2SiO_4$. Contrib Mineral Petr 123:345–357. https://doi.org/10.1007/s004100050161

Koshlyakova NN, Zubkova NV, Pekov IV et al (2017) Crystal chemistry of vanadate garnets from old metallurgical slags Lavrion, Greece. J Min Geochem 194:19–25. https://doi.org/10.1127/njma/2016/0010

Kroll H, Schmid-Beurmann P, Sell A, Büscher J, Dohr R, Kirfel A (2019) Thermal expansion and thermal pressure in Co and Ni olivines: a comparison with Mn and Fe olivines. Eur J Mineral 31:313–324. https://doi.org/10.1127/ejm/2019/0031-2805

Lin CC (2001a) High-pressure Raman spectroscopic study of Co- and Ni-olivines. Phys Chem Min 28:249–257. https://doi.org/10.1007/s002690100158

Lin CC (2001b) Vibrational spectroscopic study of the system α-Co_2SiO_4-α-Ni_2SiO_4. J Sol State Chem 157(1):102–109. https://doi.org/10.1006/jssc.2000.9044

Liu L, Mernagh TP (1994) Raman Spectra of high-pressure polymorphs of Mg_2SiO_4 at various temperatures. High Temp-High Press 26:631–637

Liu L, Lin CC, Mernagh TP, Inoue T (2002) Raman spectra of hydrous γ -Mg_2SiO_4 at various pressures and temperatures. Phys Chem Min 29:181–187. https://doi.org/10.1007/s00269-001-0219-1

Liu D, Pang Y, Ye Y, Jin Z, Symth JR, Yang Y, Zhang Z, Wang Z (2019) In-situ high-temperature vibrational spectra for synthetic and natural clinohumite: implications for dense hydrous magnesium silicates in subduction zones. Am Min 104(1):53–63. https://doi.org/10.2138/am-2019-6604

Liu D, Guo X, Symth JR, Wang X, Zhu X, Miao Y, Bai J, Ye Y (2021) High-temperature and high-pressure Raman spectra of $Fo_{89}Fa_{11}$ and $Fo_{58}Fa_{42}$ olivines: iron effect on thermodynamic properties. Am Min 106(10):1668–1678. https://doi.org/10.2138/am-2021-7686

Ma CB (1974) Reinvestigation of the olivine-spinel transformation in Ni_2SiO_4 and the incongruent melting of Ni_2SiO_4 olivine. J Geophys Res 79(23):3321–3324. https://doi.org/10.1029/JB079i023p03321

Mao HK, Takahashi T, Bassett WA (1970) Isothermal compression of the spinel phase of Ni_2SiO_4 up to 300 kilobars at room temperature. Phys Earth Planet Inter 3:51–53. https://doi.org/10.1016/0031-9201(70)90043-9

Matzen AK, Baker MB, Beckett JR, Stolper EM (2013) The temperature and pressure dependence of nickel partitioning between olivine and silicate melt. J Petrol 54(12):2521–2545. https://doi.org/10.1093/petrology/egt055

McDonough WF (2014) Compositional model for the earth's core. In: Holland HD, Turekian KK (eds) Treatise on Geochemistry, 2nd edn. Elsevier, Oxford, pp 559–577. https://doi.org/10.1016/B978-0-08-095975-7.00215-1.

McKeown DA, Bell MI, Caracas R (2010) Theoretical determination of the Raman spectra of single-crystal forsterite (Mg_2SiO_4). Am Min 95(7):980–986. https://doi.org/10.2138/am.2010.3423

Palme H, O'Neill H (2014) Cosmochemical estimates of mantle composition. In: Holland HD, Turekian KK (eds) Treatise on Geochemistry, 2nd edn. Elsevier, Oxford, pp 1–39. https://doi.org/10.1016/B978-0-08-095975-7.00201-1

Prince E (2004) In: Prince E (ed) International tables for crystallography, volume C: mathematical physical and chemical tables, 3rd edn. Springer, Dordrecht, the Netherlands. https://doi.org/10.1107/97809553602060000103

Pu X, Lange RA, Moore G (2017) A comparison of olivine-melt thermometers based on D_{Mg} and D_{Ni}: the effects of melt composition, temperature, and pressure with applications to MORBs and hydrous arc basalts. Am Min 102(4):750–765. https://doi.org/10.2138/am-2017-5879

Putirka K, Tao Y, Hari KR, Perfit MR, Jackson MG, Arevalo R (2018) The mantle source of thermal plumes: Trace and minor elements in olivine and major oxides of primitive liquids (and why the olivine compositions don't matter). Am Min 103(8):1253–1270. https://doi.org/10.2138/am-2018-6192

Redfern S, Artioli G, Rinaldi R, Henderson CMB, Knight KS, Wood BJ (2000) Octahedral cation ordering in olivine at high temperature. II: an in situ neutron powder diffraction study on synthetic $MgFeSiO_4$ (Fa50). Phys Chem Min 27:630–637. https://doi.org/10.1007/s002690000109

Ringwood AE, Major A (1970) The system Mg_2SiO_4-Fe_2SiO_4 at high pressures and temperatures. Phys Earth Planet Inter 3:89–108. https://doi.org/10.1016/0031-9201(70)90046-4

Sato Y (1977) Equation of state of mantle minerals determined through high-pressure X-ray study. High Press Res 307–323. https://doi.org/10.1016/B978-0-12-468750-9.50028-0

Sheldrick GM (2015) Crystal structure refinement with SHELXL. Acta Crystallogr C 71(1):3–8. https://doi.org/10.1107/S2053229614024218

Straub SM, LaGatta AB, Pozzo ALMD, Langmuir CH (2008) Evidence from high-Ni olivines for a hybridized peridotite/pyroxenite source for orogenic andesites from the central Mexican Volcanic Belt. Geochem Geophys Geosyst 9(3):Q03007. https://doi.org/10.1029/2007GC001583

Tredoux M, de Wit MJ, Hart RJ, Armstrong RA, Lindsay NM, Sellschop JPF (1989) Platinum group elements in a 3.5 Ga nickel-iron occurrence: possible evidence of a deep mantle origin. J Geophys Res 94(B1):795–813. https://doi.org/10.1029/JB094iB01p00795

Yamanaka T, Ishii M (1986) Raman scattering and lattice vibrations of Ni_2SiO_4 spinel at elevated temperature. Phys Chem Min 13:156–160. https://doi.org/10.1007/BF00308157

Yang Y, Wang Z, Smyth JR, Liu J, Xia Q (2015) Water effects on the anharmonic properties of forsterite. Am Min 100(10):2185–2190. https://doi.org/10.2138/am-2015-5241

Yang M, Cheng X, Li Y, Ren Y, Liu M, Qi Z (2017) Anharmonicity of monolayer MoS_2, $MoSe_2$, and WSe_2: a Raman study under high pressure and elevated temperature. Appl Phys Lett 110(9):093108. https://doi.org/10.1063/1.4977877

Zhai K, Xue W, Wang H, Wu X, Zhai S (2020) Raman spectra of sillimanite, andalusite, and kyanite at various temperatures. Phys Chem Min 47:23. https://doi.org/10.1007/s00269-020-01092-9

Zhang L, Smyth JR (2022) Crystal chemistry of metal element substitution in olivine and its high-pressure polymorphs: implications for the upper-mantle and the mantle transition zone. Earth-Sci Rev 232:104127. https://doi.org/10.1016/j.earscirev.2022.104127

Zhang L, Smyth JR, Kawazoe T, Jacobsen SD, Qin S (2018) Transition metals in the transition zone: partitioning of Ni, Co, and zn between olivine, wadsleyite, ringwoodite, and clinoenstatite. Contrib Mineral Petr 173:52. https://doi.org/10.1007/s00410-018-1478-x

Zhang D, Hu Y, Xu J, Downs RT, Hammer JE, Dera PK (2019) High-pressure behavior of liebenbergite: the most incompressible olivine-structured silicate. Am Min 104(4):580–587. https://doi.org/10.2138/am-2019-6680